



UNIVERSITY OF LEEDS

This is a repository copy of *Bubble-Driven Detachment of Bacteria from Confined Microgeometries*.

White Rose Research Online URL for this paper:
<http://eprints.whiterose.ac.uk/158296/>

Version: Accepted Version

Article:

Khodaparast, S, Kim, MK, Silpe, JE et al. (1 more author) (2017) Bubble-Driven Detachment of Bacteria from Confined Microgeometries. *Environmental Science & Technology*, 51 (3). pp. 1340-1347. ISSN 0013-936X

<https://doi.org/10.1021/acs.est.6b04369>

© 2017 American Chemical Society. This is an author produced version of a paper published in *Environmental Science & Technology*. Uploaded in accordance with the publisher's self-archiving policy.

Reuse

Items deposited in White Rose Research Online are protected by copyright, with all rights reserved unless indicated otherwise. They may be downloaded and/or printed for private study, or other acts as permitted by national copyright laws. The publisher or other rights holders may allow further reproduction and re-use of the full text version. This is indicated by the licence information on the White Rose Research Online record for the item.

Takedown

If you consider content in White Rose Research Online to be in breach of UK law, please notify us by emailing eprints@whiterose.ac.uk including the URL of the record and the reason for the withdrawal request.



eprints@whiterose.ac.uk
<https://eprints.whiterose.ac.uk/>

Bubble-driven detachment of bacteria from confined micro-geometries

Sepideh Khodaparast,[†] MinYoung K. Kim,[‡] Justin Silpe,[‡] and Howard A. Stone^{*,†}

[†]*Department of Mechanical and Aerospace Engineering, Princeton University, Princeton, NJ 08544*

[‡]*Department of Molecular Biology, Princeton University, Princeton, NJ 08544*

E-mail: hastone@princeton.edu

Phone: +1 (609) 258-9493. Fax: +1 (609) 258-6109

Abstract

Moving air-liquid interfaces, e.g. bubbles, play a significant role in the detachment and transport of colloids and microorganisms in confined systems as well as unsaturated porous media. Moreover, they can effectively prevent and/or postpone the development of mature biofilms on surfaces that are exposed to bacteria. Here we demonstrate the dynamics and quantify the effectiveness of this bubble-driven detachment process for the bacterial strain *Staphylococcus aureus*. We investigate the effects of interface velocity and geometrical factors through microfluidic experiments that mimic some of the confinement features of pore-scale geometries. Depending on the bubble velocity U , at least three different flow regimes are found. These operating flow regimes not only affect the efficiency of the detachment process but also modify the final distribution of the bacteria on the surface. We organize our results according to the capillary number, $Ca = \frac{\mu U}{\gamma}$, where μ and γ are the viscosity and the surface

tension, respectively. In particular, bubbles at very low velocities, corresponding to capillary numbers $Ca < 5 \times 10^{-5}$, exhibit detachment efficiencies of up to 80% at the early stage of bacterial adhesion. In contrast, faster bubbles at capillary numbers $Ca > 10^{-3}$, have lower detachment efficiencies and cause significant non-uniformities in the final distribution of the cells on the substrate. This effect is associated with the formation of a thin liquid film around the bubble at higher Ca . In general, at higher bubble velocities bacterial cells in the corners of the geometry are less influenced by the bubble passage compared to the central region.

Introduction

Air-liquid interfaces are known to be effective in removing dust and micron-sized contamination from solid substrates.¹⁻⁴ An inspiring example of this phenomenon is the natural self cleaning process observed in leaves of the plant *Nelumbo nucifera* in the presence of rolling water droplets.^{5,6} Such a cleaning process is affected by a strong capillary force generated as the moving air-liquid interface comes in contact with the particles attached to the surface.⁷ Similar concepts have been successfully applied in froth filtration and water purification,⁸⁻¹⁰ de-inking processes,¹¹ and cleansing of semiconductors for microelectronics.⁸ In this paper, we explore the potential of this phenomenon for removing bacteria from solid substrates.

Many other examples of colloidal detachment and transport stimulated by moving air-liquid interfaces occur in confined geometries.¹²⁻¹⁵ For example, imbibition or drainage can mobilize substantial amounts of colloidal particles and contamination within unsaturated porous media, such as the vadose zone^{12,16-18} and, therefore, are of great importance in environmental protection and remediation. Similarly, air-liquid interfaces can detach, transport and relocate microorganisms in unsaturated porous media.¹⁹⁻²² Transport of bacteria in unsaturated soil and aquifers is of great importance in in-situ biodegradation, biofacilitated transport of pollutants,^{23,24} and dispersal of pathogenic microorganisms,²⁵ which can significantly influence the underground water quality.

This mechanism may also be employed for cleaning industrial and medical surfaces and pores contaminated with initially adhering bacterial cells and, consequently, can prevent or postpone the formation and development of mature biofilms.^{26–30}

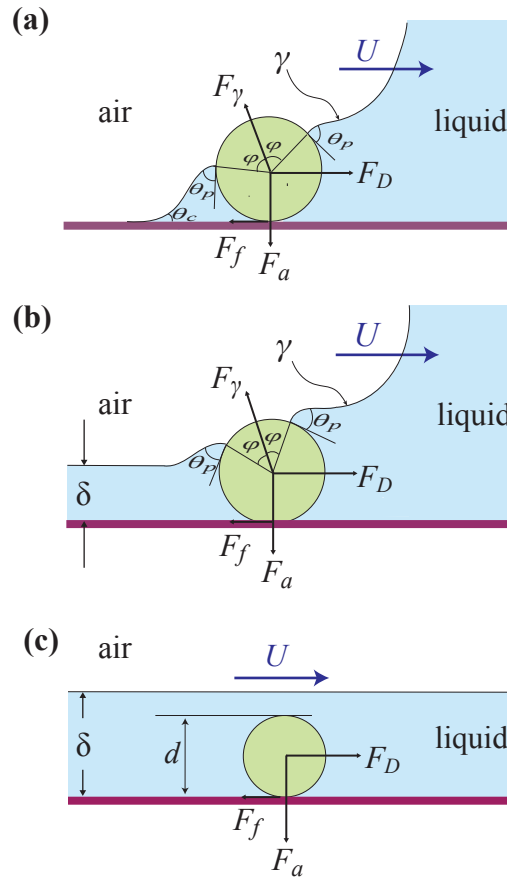


Figure 1: Schematic of the forces acting on a spherical particle of diameter d resting on a solid substrate in the vicinity of a moving air/liquid interface. (a) The liquid film thickness δ is negligible, $\delta \ll d$, (b) the liquid film thickness is comparable to the particle diameter, $\delta \approx d$, and (c) the liquid film thickness is larger than the particle diameter, $\delta > d$. Here U represents the typical speed of the bubble and γ is the surface tension. θ_c , θ_p and ϕ stand for the contact angles on the substrate and the particles and the filling angle, respectively. Forces acting on the particle are denoted as F_D (drag force), F_f (friction force), F_γ (surface tension force) and F_a (adhesion force). Note that the direction and the magnitude of F_γ depend on the filling angle ϕ and the contact angle on the particle θ_p .

An efficient capillary detachment process involves local blocking of the contact line by adhering particles, subsequent thinning of the liquid film that is formed between the interface and the

particle, the rupture of the liquid film and finally formation of a stable three-phase contact line;⁴ see Figure 1a. The capillary force can be predicted based on the surface tension of the working liquid γ and the liquid contact angle on the particle θ_p , i.e. $F_\gamma = 2\pi d\gamma\sin\phi\sin(\theta_p - \phi)$, where d is the particle diameter and ϕ is the so-called filling angle; see the schematic in Figure 1. Force balance studies have proved that the capillary induced lift force can potentially overcome by orders of magnitude the adhesion force keeping the micron-sized colloids on the substrate.^{1,7,12,31} For live microorganisms such as bacteria, however, the necessary force for successful detachment measured in experiments is often orders of magnitude larger than the theoretical prediction of the adhesion force.³² This can be due to the enhanced adhesion of bacteria on the surface caused by the shear stress of the flow^{33–35} and polymeric interactions between the surface of bacteria and the substrate.³⁶

The capillary detachment is expected to be effective when F_γ overcomes the adhesion force F_a (Figure 1). A convenient measure of the effectiveness of a detachment process is provided by the detachment efficiency,

$$\eta_{ca} = \frac{\# \text{ colloids before} - \# \text{ colloids after}}{\# \text{ colloids before}} \times 100 \quad (1)$$

Previous experimental studies have often reported overestimation of the detachment efficiency η_{ca} by theoretical analyses from which the minimum force required for the detachment of a spherical particle is calculated based on the DLVO theory. Dynamic flow parameters, often neglected in the theoretical calculations, are suspected to be the main reason behind these discrepancies. Indeed, multiple experimental investigations have reported noticeable effects of flow parameters, especially the interface velocity U , on the final detachment efficiency of both micron-sized particles and microorganisms.^{2,4,37,38} A summary of these studies and their concluding remarks on the effect of the interface velocity U are presented in Table 1. In general, it has been often observed that increasing the interface velocity reduces the detachment efficiency η_{ca} . This result has been

suggested to be caused by insufficient contact time between the interface and the particle at higher velocities and the resulting inefficiency of the detachment process.^{3,4,37} However, Aramrak et al. (2011) showed that even at the highest interface velocities in their experiments the contact time between the particle and the interface is larger than 10^{-2} ms for a particle of $1 \mu\text{m}$ diameter, which they suggest is orders of magnitude larger than the required time for the formation of the three-phase contact line. Therefore, as they suggest the contact time in the range of velocities covered in most of the previous experiments is not the limiting factor in the capillary detachment process, and the influence of interface velocity on the final result is probably due the formation of a thin liquid film on the solid wall (Figure 1b).¹³ This effect is expected to be enhanced as the liquid film becomes thicker than the size of the particles and direct capillary forces are no longer applicable (Figure 1c). The main goal of this study is to visualize and quantify the effect of the interface velocity and the liquid film thickness on the efficiency of the capillary detachment of bacteria adhered to a surface.

Natural and engineered unsaturated porous media, as well as laboratory experiments, often involve confined geometries.³⁹ In such geometries, the gas-liquid interface may no longer form a contact line on the solid substrate. In fact, it is well known that in confined geometries, such as microfluidic channels, and in the absence of inertial and buoyancy effects, a moving gas-liquid interface, e.g. a bubble, leaves a liquid film on the wall, whose thickness δ is determined by the pore size and the interplay between the surface tension γ and the viscous forces, which is quantified by the capillary number,^{40,41} $Ca = \frac{\mu U}{\gamma}$, where μ the liquid viscosity and U is the bubble velocity. Often the capillary number is very small $Ca \ll 1$ and the thickness of the liquid film is much smaller than the bubble radius. Despite their potential significance in the capillary detachment process, the confinement effects and the presence of the thin lubrication film at the pore walls has been so far overlooked in both theoretical analyses and interpretation of experimental observations.

In this work, we show an effect of the lubricating liquid film around long bubbles on the efficiency of capillary detachment in microfluidic channels. Since the film thickness depends on

the channel dimensions and the capillary number, as will be discussed later in detail, we study different channel heights H and aspect ratios A_R of channel cross-section, and a wide range of capillary numbers. Experiments are performed with nearly spherical bacteria, *Staphylococcus aureus*. Quantification and understanding of this problem will be based on simultaneous and dynamic tracking of the moving interface and the microorganisms. To this end, we use fluorescent and high-speed bright-field microscopy to visualize the dynamic mechanism of detachment in the presence of a liquid film and quantify the detachment efficiency for different bubble velocities and channel dimensions.

Experiments

Microfluidic devices

In order to study a model for the confinement where the bubble size is comparable to the pore space, we used microfluidic channels with rectangular cross-sections. We use three different microfluidic channels in our experiments: (Channel A) $250\ \mu\text{m} \times 250\ \mu\text{m} \times 30\ \text{mm}$ ($W \times H \times L$), (Channel B) $100\ \mu\text{m} \times 100\ \mu\text{m} \times 30\ \text{mm}$ ($W \times H \times L$), and (Channel C) $500\ \mu\text{m} \times 100\ \mu\text{m} \times 30\ \text{mm}$ ($W \times H \times L$). These designs allowed us to study two different channel heights H and two different aspect ratios $A_R = 1, 5$. In order to generate a host-like surface that bacteria often encounter, surfaces of all the channels were pre-treated with air plasma and coated with $50\ \mu\text{g/ml}$ fibronectin solution from human plasma, as previously described.⁴³ This step enhances the adhesion probability of the *Staphylococcus aureus* on the surface because *S. aureus* has specific fibronectin-binding proteins on the cell surface.^{43,44} The measured contact angle of the working fluid on the coated substrates was $\theta_c = 37^\circ \pm 5^\circ$ (Supporting Information).

Table 1: Previous research

Ref.	Ca^*	Geometry	Particles**	Regime***	Remarks
13	10^{-8} - 10^{-4}	circular, $R = 1.35 \text{ mm}$	hydrophilic, $d = 1 \mu\text{m}$	1 to 3	η_{ca} increases with decreasing Ca .
37	10^{-5} - 10^{-4}	rectangular, $H = 0.6 \text{ mm}$, $W = 5 \text{ mm}$	polystyrene, $d = 0.8 \mu\text{m}$	1 and 2	η_{ca} increases linearly with decreasing Ca .
38	10^{-5} - 10^{-4}	rectangular, $H = 0.6 \text{ mm}$, $W = 5 \text{ mm}$	bacterial cells, different sizes	1 and 2	η_{ca} increases with decreasing Ca .
42	1.2×10^{-7}	rectangular, $H = 0.4 \text{ mm}$, $W = 3.8 \text{ mm}$	polystyrene, $d = 1 \mu\text{m}$	1	Proposed theory in the article overestimates the experimental η_{ca} .
7	$\simeq 10^{-4}$	rectangular, $H = 0.6 \text{ mm}$, $W = 5 \text{ mm}$	polystyrene, $d = 0.817 \mu\text{m}$	2	Proposed theory in the article overestimates the experimental η_{ca} .

* The capillary number Ca is calculated based on the interface velocity U provided in the articles. ** Polystyrene particles used in some of the studies had modified surfaces. *** This column refers to the operating regime predicted based on the present observations described in the Results Section. Estimates are based on Ca and the average ‘Bretherton’ film thickness relative to the diameter of colloids/bacteria d used in each study.

Bacteria strain and culture condition

As *S. aureus*, a notorious human pathogen, causes some of the most common biofilm related infections, and is resistant to many antibiotics, we study this bacteria to investigate the potential of a new strategy for preventing and/or removing biofilms. Moreover, *S. aureus* exhibits several advantageous features for our study: (1) They are not motile and have an approximately spherical shape, which minimize the complications caused by shape factors.³⁸ (2) The size of the bacterium ($\approx 1 \mu\text{m}$ diameter) falls in the range where for colloidal particles the capillary detachment process becomes important and efficient.² (3) Preliminary tests and earlier studies with *S. aureus* showed that capillary detachment can overcome the adhesion energy of these bacterial cells.²⁷ *S. aureus* strain RN6734 was used in this study and throughout our paper is always indicated as *S. aureus*. In order to make a strain that fluoresces at a constant level, we constructed a plasmid carrying a constitutively expressing mKO (Supporting Information). *S. aureus* strain was grown overnight at 37°C with shaking in Tryptic Soy Broth (TSB) with $10 \mu\text{g/ml}$ erythromycin to maintain plasmids, back-diluted 1:1000 and re-grown for 3 hours to $\text{OD}_{600} \simeq 0.2$. The measured contact angle of the working liquid on the lawns of *S. aureus* created from the suspensions was $\theta_p = 14^\circ \pm 2^\circ$ (Supporting Information).

Visualization and quantification

Bright-field imaging was performed with a high-speed camera with frame rates up to 4000 fps for tracking the dynamics of the interaction between the bacteria and the interface, while fluorescent microscopy was used for cell-counting before and after the passage of the bubbles. The focal plane of a 40X dry objective was set on the bottom wall of the microchannels, where bacterial cells are deposited. Images covered a length of $350 \mu\text{m}$ and the entire width of the channels. To measure the number of the adhering cells on the substrate, before and after the passage of bubbles, the constitutive mKO fluorescence captured from the total area was summed and divided by the

experimentally determined average fluorescent signal of single cells. The detachment efficiency for every bubble in the sequence is calculated based on the initial number of the bacteria before the first bubble passes.

Experimental procedure

Channels were loaded with bacterial cultures for 30 minutes with an average speed of approximately $250 \mu\text{m/s}$ after which sterile minimal growth medium was flowed steadily for 15 minutes into the device to remove unattached planktonic cells. The average surface density of bacterial cells adhering on the substrate was around 15000 cells/mm^2 at this stage. We then inject bubbles of length L_b in a channel of height H (Figure 2a). In particular, a sequence of four long bubbles ($\frac{L_b}{H} > 50$) is injected far upstream of the measurement point. The bubbles were carried by the liquid phase into the microchannel. The flow into the main channel was driven using a syringe pump at a constant flow rate Q , where $0.1 \mu\text{l/min} < Q < 1000 \mu\text{l/min}$ corresponding to $10^{-6} < Ca < 10^{-2}$ based on the properties of the working fluid (Figure S1). The surface tension and viscosity of the working fluid were 0.072 N/m and 0.001 Pa.s , respectively. Videos of example cases, including the status of bacteria attached to the substrate before and after the bubble passes, can be found in the Supporting Information.

Moving air-liquid interfaces in confined geometries

The interplay between the capillary force, induced by a moving interface, and the adhesion force acting on the particles determines the efficiency of the capillary detachment process (Figure 1). Theoretical analyses of the detachment of colloidal particles/bacteria adhering to solid substrates in the presence of an air-liquid interface have been reported in several previous studies,^{7,13,38} though our goal is not to measure the adhesion but rather to document the influence of flow and film thickness on the removal process. It should be noted that for bacteria, interactions between the cell

surface polymers and the substrate, and the flow-induced shear stress may significantly modify the adhesion energy compared to the extended DLVO interaction energy predictions,^{45,46} and thus, theoretical calculations tend to fail in predicting the required minimum capillary force for successful detachment of bacteria to occur.³² This fact further increases the complexity of the problem and necessitates accurate experimental measurements to achieve realistic understanding.

For a substrate exposed to a flow containing bubbles rather than a stagnant fluid, the deposited colloidal particles/bacteria on the surface are exposed to a moving air-liquid interface. The motion of the interface not only induces a viscous drag force on the particle but also leaves a thin liquid film between the gas-liquid interface and the bounding walls of the confined geometry. Until now effect of this thin film has been assumed to be negligible in the analyses provided in the literature, however, it has been postulated recently to be the reason behind the common theoretical overestimation of colloid detachment efficiency.⁴² In fact, in a confined geometry the problem of interest is no longer a moving contact line problem but instead is a classic “Bretherton” problem of a bubble translating in a close-fitting channel with walls covered with micron-sized colloids. As a gas phase moves into a tube otherwise filled with wetting liquid, it does not create a contact line on the wall but instead the gas-liquid interface is separated from the wall by a uniform thin liquid film.^{40,41,47} For a finite volume of gas, this interface forms a bubble with a curved nose and back, see Figure 2a.

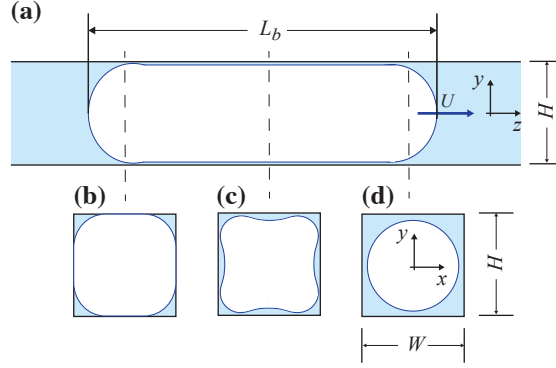


Figure 2: Flow of an elongated confined bubble of length L_b in a channel of square cross section. (a) Side view of the flow. (b) Cross-sectional view close to the rear end of the bubble. (c) The middle region. (d) View close to the front nose of the bubble.

The dynamics of the bubble are characterized by the capillary number, Ca . In a tube of circular cross-section of radius R and at low interface velocities, i.e., $Ca \ll 1$, the thickness of the liquid layer δ is determined by the interplay between the viscous and the surface tension forces and can be estimated as follows:⁴⁰

$$\frac{\delta}{R} = 1.34 Ca^{2/3} \quad (2)$$

For example, for a typical value of $Ca = 10^{-3}$, then $\frac{\delta}{R} \simeq 0.01$. We demonstrate below the impact of such thin films on bacterial detachment. In a channel with rectangular cross-section, this liquid film is no longer uniformly distributed around the bubble though the film thickness has the order of magnitude given by Equation 2.⁴⁸ Instead, corners of the channel are filled with liquid, while the bubble fills the centre of the opening, and the film thickness depends on the circumferential and the axial coordinates (Figure 2b-d).^{48,49} For a partially wetting liquid, the liquid film may eventually dry out towards the back of the bubble,⁵⁰ as illustrated schematically in Figure 2a. Therefore, depending on their location, the colloidal particles/bacteria on the walls of channel or small pores may experience one or multiple cases of the three scenarios illustrated in Figure 1. Only those particle/bacteria that come in contact with an air-liquid interface experience the direct capillary

detachment force.

In order to achieve all the three cases schematically presented in Figure 1, a wide range of flow capillary numbers, $10^{-6} < Ca < 2 \times 10^{-3}$, are covered in our experiments. As an example, in channel A and for $10^{-6} < Ca < 2 \times 10^{-3}$, the average film thickness predictions varies between tens of nanometers ($\delta \ll d$) to a few micrometers ($\delta > d$). These predictions are obtained using channel height H in place of R in Equation 2 for normalizing the film thickness.

Results and discussion

We report the results of our observations as a function of capillary number and channel dimensions. Bacterial cell counting is performed before and after every bubble for a sequence of four bubbles at each capillary number. For the experiments discussed here, the total detachment efficiency was observed not to increase when increasing the number of bubbles above four. Detachment efficiencies presented in all of the figures are the average value of three independent measurements obtained from separately grown bacterial strains, and the error bars present the standard errors calculated for these measurements. We note that no bacteria were detached due to the single-phase shear stress induced by the liquid phase in the absence of the bubbles.

Capillary number

Detachment efficiencies for a representative set of experiments in channel A, after the first and fourth bubbles pass through the channel, are presented in Figure 3. Based on the dynamic tracking of the interface and its interaction with the bacteria adhering on the substrate, at least three distinct regimes were observed. Different regimes are defined based on the ratio of the bacteria diameter to the liquid film thickness $\frac{d}{\delta}$, which is a function of the flow Capillary number for a given channel height.

Regime 1 ($Ca < 5 \times 10^{-5}$). In this regime, the thin liquid film at the nose of the bubble

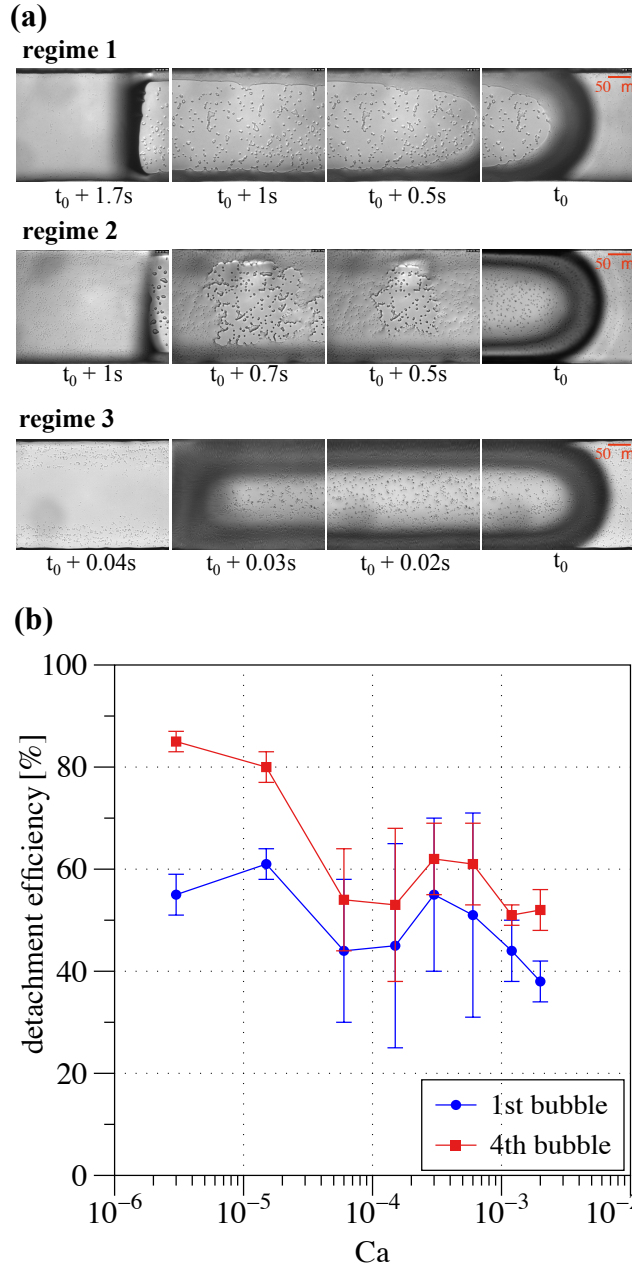


Figure 3: Different regimes observed in the capillary detachment process in channel A, $H = 250 \mu\text{m}$. (a) Examples of air-liquid interfaces, in the form of a confined bubble, interacting with the bacteria in regime 1 at $Ca = 3 \times 10^{-6}$, regime 2 at $Ca = 1.5 \times 10^{-4}$, and regime 3 at $Ca = 2 \times 10^{-3}$. Flow direction is from left to the right. The images are taken at a fixed location in the channel as the bubbles pass. Visualizations are performed in the bright-field mode to demonstrate the interaction of the interface with the bacteria and the dry-out patterns. (b) Detachment efficiency (Equation 1) based on the initial number of bacteria versus capillary number after the first and the fourth bubbles pass.

immediately dries out and creates a contact line covering almost the entire width of the channel, which acts effectively in cleaning the surface, see Figure 3a. This consistent dry-out pattern results in small error bars in the measurement of the detachment efficiency at $Ca < 5 \times 10^{-5}$. The liquid film thickness in this regime is expected to be negligible compared to the size of the bacterial cells and thus this regime is expected to result in detachment efficiencies close to 100%. However, flow visualization of the film shape reveals several structures as the main reasons behind the reduced efficiency values presented in Figure 3b for $Ca < 5 \times 10^{-5}$: (i) As schematically illustrated in Figure 2, bubbles do not fill the entire cross section of the channel, and, therefore, bacteria in the corner regions are not mobilized. We refer to this feature as the *corner effect* in the rest of the text. (ii) Although the liquid film dries out in the central zone, liquid patches are observed to remain on the surface (Figure 3a). Some of the bacteria in these sites are mobilized and eventually removed by the back of the bubble, while the rest remain adhered on the substrate. The adhering bacteria are believed to be responsible for keeping the liquid patches on the substrate, since no similar flow pattern was observed at identical capillary numbers and surface conditions with no bacteria. (iii) The dewetting of the film hinders the motion of the bubble as was also reported in previous investigations.⁵¹ As the result, the back of the bubble goes through pinning and de-pinning motions, which causes re-deposition of some bacteria at the pinning sites. In general, the bacteria remaining on the surface have an approximately uniform distribution on the wall except from the corner regions and increasing the number of bubbles enhances the detachment efficiency in this regime.

Regime 2 and 3. Although the detachment efficiencies presented in Figure 3b seem quite similar for $Ca > 5 \times 10^{-5}$, dynamic tracking of the interface and its interaction with bacteria suggests two distinct detachment mechanisms, which we refer to as regime 2 ($5 \times 10^{-5} < Ca < 10^{-3}$), and regime 3 ($Ca > 10^{-3}$). In summary, the most significant features of these two regimes are:

Regime 2 ($5 \times 10^{-5} < Ca < 10^{-3}$). The liquid film at the nose of the bubble in this regime is too thick to dry out immediately. However, eventually, due to its three-dimensional distribution

around the bubble and the disturbances on the surface,⁵² caused by the adhering bacteria, the film ruptures farther downstream. The resulting contact line appears to move only slowly in the flow direction and mostly moves towards the channel wall (see Figure 3a, regime 2). This effect is observed to push the bacteria towards the channel side walls, which are the regions less accessible to the contact line. Together with the wider liquid-filled corners, the irregular dry-out patterns in this regime reduce the detachment efficiency down to less than 50% when compared to regime 1. The final distribution and quantity of bacteria on the surface are determined by the dewetting pattern. The dewetting patterns are dependent on the contact angle of the working fluid on the substrate and on the bacteria, cell concentration on the substrate, and the channel geometry. Investigations on the effect of these parameters require further extensive studies which are beyond the scope of the present work. Regime 2 has the lowest detachment efficiency compared to the other regimes, and passing more bubbles seems to only slightly enhance the detachment efficiency, while redistributing the non-detached bacteria on the substrate.

Regimes 1 and 2 both fall within the *wedging flow* category as described by Cubaud et al. (2004). Global dry-out patterns starting from the nose or local dry-out patterns starting farther from the bubble nose were observed by the authors at the lower velocities for partially wetting liquids, which is qualitatively in agreement with the present observations. Moreover, our estimate of the film thickness based on the Bretherton formulation for the studies summarized in Table 1 suggest that most of these measurements were performed in regimes 1 and 2.

Regime 3 ($Ca > 10^{-3}$). The main characteristic of this regime is the presence of a continuous liquid film. The final distribution and quantity of the bacteria on the substrate were consistent for all the experiments. For $Ca > 10^{-3}$, the central region of the channel wall, shadowed by the bubble, is perfectly clean, while the bacteria in the corners remain almost untouched, see Figure 3a, regime 3. The liquid-filled corners at such capillary numbers are wider and fill almost 50% of the channel width. The 50% detachment efficiency in this regime, as shown in Figure 3b, demonstrates that the bubble is almost 100% efficient in cleaning the central zone of the wall. High-speed flow

visualizations show that bacteria were initially removed in two stripes parallel to the flow direction where the film starts to leak towards the corners (see the schematic in Figure 2c and d). These stripes then merge towards the back of the bubble due to the thinning of the liquid film, as predicted previously.^{48,49} As the bacteria are washed away from the central part of the wall, bubbles tend to dry out in this zone and detach more bacteria. Increasing the number of bubbles, however, does not improve the detachment efficiency. In the central region of the channel, bubbles are more efficient surface cleaners when operating in regime 3 compared to regimes 1 and 2. Increasing capillary numbers in this regime decreases the detachment efficiency, which is due to the thicker liquid film at the back of the bubble at higher velocities.

Channel height

Detachment efficiencies versus capillary number Ca for channel B ($H = 100 \mu\text{m}$) follows a very similar trend to that of the channel A ($H = 250 \mu\text{m}$), see Figure 4a. Since the channel height is more than two times smaller than the previous case, the average film thickness is expected to be relatively smaller than that in channel A at similar capillary numbers. In fact, we observed in the visualizations that $Ca = 5 \times 10^{-5}$ falls within regime 1 in this channel and exhibits higher detachment efficiencies, whilst in channel A flow at a similar capillary number was in regime 2. Regime 2 was observed to be less efficient in the smaller channel. Bubbles in regime 3 in channel B were, however, almost as efficient as those in channel A in cleaning the surface.

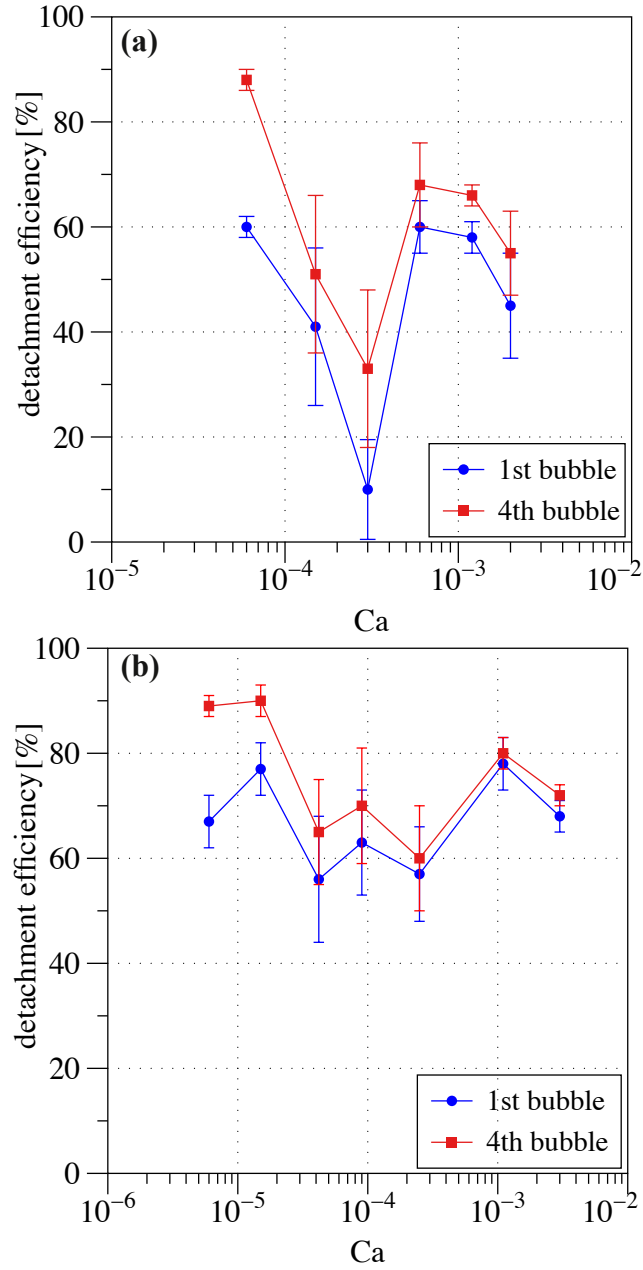


Figure 4: Detachment efficiency versus capillary number after the first and the fourth bubbles in (a) channel B ($H = 100 \mu\text{m}, A_R = 1$), and (b) channel C ($H = 100 \mu\text{m}, A_R = 5$).

Channel aspect ratio A_R

Unlike the square cross sections of channels A and B, channel C had a rectangular cross-section of aspect ratio $A_R = \frac{W}{H} = 5$. The main distinct characteristic of the flow in this channel is the narrow liquid-filled corners relative to the channel width, when compared to channels A and B. As a result, the detachment efficiencies measured in this channel were in general higher, see Figure 4b. This effect is amplified in regime 3, where the only bacteria left on the substrate after the bubble are located in the corner regions. In regime 2, bubbles were observed to be more efficient in detachment of bacteria in this channel compared to the other channels. Although the reason behind this finding is unclear, wider channels seem to be easier to clean by bubbles at intermediate capillary numbers.

Figure 5 shows the spatial distribution (see details in the Supporting Information) of the bacteria before and after the bubble passage for representative cases in channels B and C. As can be observed in Figure 5a, bubbles are highly efficient in uniformly cleaning the channel wall in regime 1. The *corner effects* in regime 3 are only present in around 10% of the half channel width for channel C, while they occupy almost half of channel width for channel B (Figure 5b). A quantitative representation of this effect is observable when comparing the detachment efficiencies of channels B and C for $Ca > 10^{-3}$ in Figure 4. As can be seen, the detachment efficiency in regime 3 is enhanced from 50% – 60% in channel B to 70% – 80% in channel C.

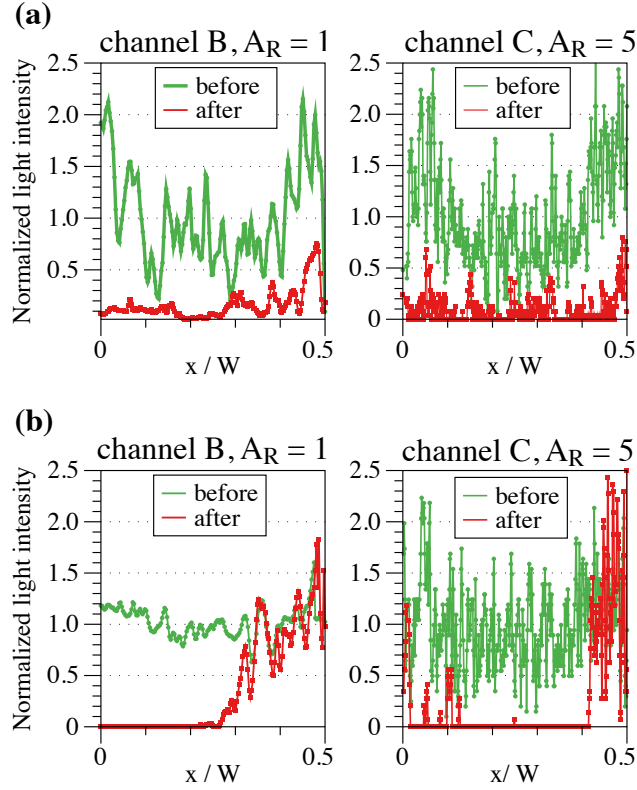


Figure 5: Sample distribution of adhering bacteria before and after the passage of the first bubble at (a) $Ca = 5 \times 10^{-5}$ (regime 1) and (b) $Ca = 10^{-3}$ (regime 3) in channels B and C. Both channels have height of $H = 100 \mu\text{m}$. Results present integrated light intensity, normalized with the average intensity before the bubble passes, captured on axial lines from the center $x/W = 0$ to the channel wall $x/W = 0.5$.

Long-term effects

Bubbles passing in microchannels were observed to detach significant quantities of bacteria from the surface even after longer exposure of the substrate to the bacterial solution (see the Supporting Information for more details of the experimental procedures). Several significant features were observed for the distribution of bacteria on the channel wall, which is exposed to bacterial solution for different duration of time up to 15 hours (see Figure S2): (i) The effect of the bubbles remains noticeable even after several hours of surface exposure to the bacterial solution. (ii) The detachment efficiency of bubbles at lower velocities ($Ca = 5 \times 10^{-5}$) decreases as we increase

the exposure time. (iii) On the contrary, the detachment efficiency increases for faster bubbles ($Ca = 10^{-3}$) as they pass over surfaces, which were subjected to adhering bacteria for a longer period. In this regime, as the thickness of the bacterial structures on the substrate increases, the probability of the contact between the bubble interface and the bacteria adhered on the substrate is increased and, therefore, bacteria are observed to be detached starting from the front nose of the bubble. Moreover, over time the bacteria start forming three-dimensional mature biofilms on the substrate. Our visualisations reveal that bubbles at higher capillary number are often capable of detaching the entire three-dimensional structures, which might be elongated from the corner zone to the central region of the pore. This effect enhances the capillary detachment in the corner regions at regime 3.

Bubbles were observed to cause notable non-homogeneous distributions of bacteria even when the substrate was exposed to the bacterial solution for several hours. As an example, Figure 6 shows the deposited bacterial cells on a channel wall before and after the passage of a bubble at $Ca \simeq 10^{-3}$. The bottom wall of the channel was exposed to bacterial solution for 8 hours before the bubble passes. The bubble removes a large number of bacteria from the central region, while its efficiency is relatively lower in the corner regions similar to the trend that was observed in the results presented earlier.

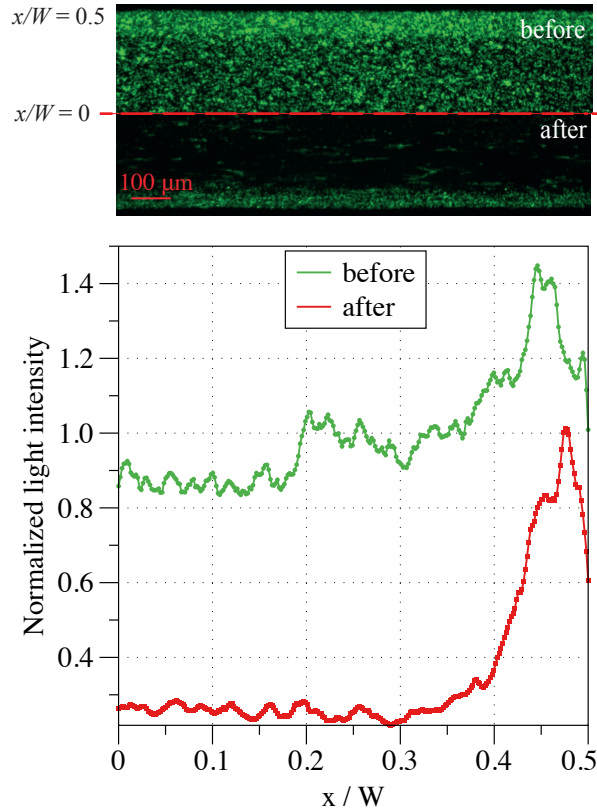


Figure 6: Distribution of bacteria adhered on the wall being exposed to bacterial solution for 8 hours before and after a bubble passes at $Ca \simeq 10^{-3}$ in channel C. Integrated light intensities are normalized with the average of the light intensity before the bubble passes. Images are captured at identical light intensities.

In summary, a direct capillary force induced by an air-liquid interface can be effective in detaching and mobilising *Staphylococcus aureus* adhered to the walls of micro channels. This phenomenon occurs at velocities where the shear stress of the flow alone at the wall has negligible effect on the adhering bacteria. Even though it has been often neglected in the previous studies, our experimental results show that the lubrication film around the bubbles in confined geometries and its interaction with the adhering bacteria have significant effects on the final detachment results. These influences are noticeable not only in the detachment efficiency but also in the final distribution of the bacteria that remain on the substrate. The observed distinct patterns in film dry-out and their direct influence on the bacterial detachment and redeposition prove that the capillary

detachment problem needs to be approached as a dynamic problem rather than a static contact line problem. The focus of the current study was on detachment of bacterial cells at their earliest stage of adhesion on the substrate, however, we also observed that bubbles are effective in cleaning surfaces that were exposed to bacteria for several hours. At the early stage of bacterial adhesion on the surface, bubbles at low velocities ($Ca < 10^{-5}$) are found to be the most efficient if maximum cleaning efficiency is desired. The present findings suggest that in confined geometries exposed to bacteria, certain locations, such as corners are more likely to be the potential zones for the formation and development of mature biofilms. Further investigations are yet to be performed to clarify the effect of substrate and bacteria surface hydrophobicity, shape, and initial cell concentration on the capillary detachment process in the presence of lubricating liquid films.

Acknowledgement

This research is supported by grant from Swiss National Science Foundation (P2ELP2-158896).

Supporting Information Available

Additional explanations, figures and videos as noted in the text can be found in the Supporting Information. This material is available free of charge via the Internet at <http://pubs.acs.org/>.

References

- (1) O'Brien, S.; Brule, B. V. D. A mathematical model for the cleansing of silicon substrates by fluid immersion. *J. Colloid Interface Sci.* **1991**, *144*, 210 – 221.
- (2) Gómez-Suárez, C.; Noordmans, J.; van der Mei, H. C.; Busscher, H. J. Removal of colloidal

- particles from quartz collector surfaces as stimulated by the passage of liquid-air interfaces. *Langmuir* **1999**, *15*, 5123–5127.
- (3) Gómez-Suárez, C.; Noordmans, J.; C. van der Mei, H.; J. Busscher, H. Detachment of colloidal particles from collector surfaces with different electrostatic charge and hydrophobicity by attachment to air bubbles in a parallel plate flow chamber. *Phys. Chem. Chem. Phys.* **1999**, *1*, 4423–4427.
- (4) Sharma, P.; Flury, M.; Zhou, J. Detachment of colloids from a solid surface by a moving air–water interface. *J. Colloid Interface Sci.* **2008**, *326*, 143 – 150.
- (5) Barthlott, W.; Neinhuis, C. Purity of the sacred lotus, or escape from contamination in biological surfaces. *Planta* **1997**, *202*, 1–8.
- (6) Solga, A.; Cerman, Z.; Striffler, B. F.; Spaeth, M.; Barthlott, W. The dream of staying clean: Lotus and biomimetic surfaces. *Bioinspir. Biomim.* **2007**, *2*, S126–34.
- (7) Noordmans, J.; Wit, P. J.; Mei, H. C. V. D.; Busscher, H. J. Detachment of polystyrene particles from collector surfaces by surface tension forces induced by air-bubble passage through a parallel plate flow chamber. *J. Adhes. Sci. Technol.* **1997**, *11*, 957–969.
- (8) Zlokarnik, M. Separation of activated sludge from purified waste water by Induced Air Flotation (IAF). *Water Res.* **1998**, *32*, 1095 – 1102.
- (9) Dai, Z.; Fornasiero, D.; Ralston, J. Particle–bubble attachment in mineral flotation. *J. Colloid Interf. Sci.* **1999**, *217*, 70 – 76.
- (10) Edzwald, J. K. Dissolved air flotation and me. *Water Res.* **2010**, *44*, 2077 – 2106.
- (11) Bloom, F.; Heindel, T. J. A theoretical model of flotation deinking efficiency. *J. Colloid Interf. Sci.* **1997**, *190*, 182 – 197.

- (12) Shang, J.; Flury, M.; Chen, G.; Zhuang, J. Impact of flow rate, water content, and capillary forces on in situ colloid mobilization during infiltration in unsaturated sediments. *Water Resour. Res.* **2008**, *44*, W06411.
- (13) Aramrak, S.; Flury, M.; Harsh, J. B. Detachment of deposited colloids by advancing and receding air–water interfaces. *Langmuir* **2011**, *27*, 9985–9993, PMID: 21714545.
- (14) Lazouskaya, V.; Jin, Y. Colloid retention at air–water interface in a capillary channel. *Colloid Surface A* **2008**, *325*, 141 – 151.
- (15) Zevi, Y.; Gao, B.; Zhang, W.; Morales, V. L.; Cakmak, M. E.; Medrano, E. A.; Sang, W.; Steenhuis, T. S. Colloid retention at the meniscus-wall contact line in an open microchannel. *Water Res.* **2012**, *46*, 295–306.
- (16) Sirivithayapakorn, S.; Keller, A. Transport of colloids in unsaturated porous media: A pore-scale observation of processes during the dissolution of air-water interface. *Water Resour. Res.* **2003**, *39*, n/a–n/a, 1346.
- (17) Zhuang, J.; McCarthy, J. F.; Tyner, J. S.; Perfect, E.; Flury, M. In situ colloid mobilization in hanford sediments under unsaturated transient flow conditions: effect of irrigation pattern. *Environ. Sci. Technol.* **2007**, *41*, 3199–3204, PMID: 17539526.
- (18) Saiers, J. E.; Hornberger, G. M.; Gower, D. B.; Herman, J. S. The role of moving air-water interfaces in colloid mobilization within the vadose zone. *Geophys. Res. Lett.* **2003**, *30*, HLS 1.
- (19) Harvey, R. W.; Garabedian, S. P. Use of colloid filtration theory in modeling movement of bacteria through a contaminated sandy aquifer. *Environ. Sci. Technol.* **1991**, *25*, 178–185.
- (20) Gao, B.; Steenhuis, T. S.; Zevi, Y.; Morales, V. L.; Nieber, J. L.; Richards, B. K.; Mc-

- Carthy, J. F.; Parlange, J.-Y. Capillary retention of colloids in unsaturated porous media. *Water Resour. Res.* **2008**, *44*, W04504.
- (21) Jamieson, R.; Gordon, R.; Sharples, K.; Stratton, G.; Madani, A. Movement and persistence of fecal bacteria in agricultural soils and subsurface drainage water: a review. *Can. Biosyst. Eng.* **2002**, *44*, 1.1–1.9.
- (22) Jin, Y.; Flury, M. Fate and transport of viruses in porous media. *Adv. Agron.* **2002**, *77*, 39 – 102.
- (23) Schäfer, A.; Ustohal, P.; Harms, H.; Stauffer, F.; Dracos, T.; Zehnder, A. J. B. Transport of bacteria in unsaturated porous media. *Journal of Contaminant Hydrology* **1998**, *33*, 149–169.
- (24) Rittmann, B. E. *In Situ Bioremediation*; Noyes Publishers, Park Ridge, NJ, 1994.
- (25) Steffan, R. J.; Sperry, K. L.; Walsh, M. T.; Vainberg, S.; Condee, C. W. Field-scale evaluation of in situ bioaugmentation for remediation of chlorinated solvents in groundwater. *Environ. Sci. Technol.* **1999**, *33*, 2771–2781.
- (26) Bos, R.; van der Mei, H. C.; Gold, J.; Busscher, H. J. Retention of bacteria on a substratum surface with micro-patterned hydrophobicity. *FEMS Microbiol. Lett.* **2000**, *189*, 311–315.
- (27) Bruinsma, G.; van der Mei, H.; Busscher, H. Bacterial adhesion to surface hydrophilic and hydrophobic contact lenses. *Biomaterials* **2001**, *22*, 3217 – 3224, Ophthalmic Special Issue.
- (28) Sharma, P. K.; Gibcus, M. J.; van der Mei, H. C.; Busscher, H. J. Microbubble-induced detachment of coadhering oral bacteria from salivary pellicles. *Eur. J. Oral Sci.* **2005**, *113*, 326–332.
- (29) Parini, M. R.; Pitt, W. G. Dynamic removal of oral biofilms by bubbles. *Colloid Surface B* **2006**, *52*, 39–46.

- (30) Crusz, S. A.; Popat, R.; Rybtke, M. T.; Camara, M.; Givskov, M.; Tolker-Nielsen, T.; Diggle, S. P.; Williams, P. Bursting the bubble on bacterial biofilms: a flow cell methodology. *Biofouling* **2012**, *28*, 835–842.
- (31) Chatterjee, N.; Lapin, S.; Flury, M. Capillary forces between sediment particles and an air–water interface. *Environ. Sci. Technol.* **2012**, *46*, 4411–4418, PMID: 22423648.
- (32) Boks, N. P.; Norde, W.; van der Mei, H. C.; Busscher, H. J. Forces involved in bacterial adhesion to hydrophilic and hydrophobic surfaces. *Microbiology* **2008**, *154*, 3122–3133.
- (33) Thomas, W. E.; Trintchina, E.; Forero, M.; Vogel, V.; Sokurenko, E. V. Bacterial Adhesion to Target Cells Enhanced by Shear Force. *Cell* **2002**, *109*, 913 – 923.
- (34) Zhu, C.; Yago, T.; Lou, J.; Zarnitsyna, V. I.; McEver, R. P. Mechanisms for Flow-Enhanced Cell Adhesion. *Ann. Biomed. Eng.* **2008**, *36*, 604–621.
- (35) Lecuyer, S.; Rusconi, R.; Shen, Y.; Forsyth, A.; Vlamakis, H.; Kolter, R.; Stone, H. A. Shear Stress Increases the Residence Time of Adhesion of *Pseudomonas aeruginosa*. *Biophys. J.* **2011**, *100*, 341 – 350.
- (36) Savage, D. C.; Fletcher, M. *Bacterial Adhesion, Mechanics and Physiological Significance*; Plenum Press, New York, 1985.
- (37) Gómez-Suárez, C.; van der Mei, H. C.; Busscher, H. Air bubble-induced detachment of positively and negatively charged polystyrene particles from collector surfaces in a parallel-plate flow chamber. *J. Adhes. Sci. Technol.* **2000**, *14*, 1527–1537.
- (38) Gómez-Suárez, C.; Busscher, H. J.; van der Mei, H. C. Analysis of bacterial detachment from substratum surfaces by the passage of air-Liquid interfaces. *Appl. Environ. Microb.* **2001**, *67*, 2531–2537.

- (39) Wan, J.; Wilson, J. L. Colloid transport in unsaturated porous media. *Water Resour. Res.* **1994**, *30*, 857–864.
- (40) Bretherton, F. P. The motion of long bubbles in tubes. *J. Fluid Mech.* **1961**, *10*, 166–188.
- (41) Taylor, G. I. Deposition of a viscous fluid on the wall of a tube. *J. Fluid Mech.* **1961**, *10*, 161–165.
- (42) Lazouskaya, V.; Wang, L.-P.; Or, D.; Wang, G.; Caplan, J. L.; Jin, Y. Colloid mobilization by fluid displacement fronts in channels. *J. Colloid Interf. Sci.* **2013**, *406*, 44–50.
- (43) Kim, M. K.; Drescher, K.; Pak, O. S.; Bassler, B. L.; Stone, H. A. Filaments in curved streamlines: rapid formation of *Staphylococcus aureus* biofilm streamers. *New J. Phys.* **2014**, *16*, 065024.
- (44) Mohammad, S. F.; Topham, N. S.; Burns, G. L.; Olsen, D. B. Enhanced bacterial adhesion on surfaces pretreated with fibrinogen and fibronectin. *ASAIO Trans.* **1988**, *34*, 573–577.
- (45) Jucker, B. A.; Zehnder, A. J. B.; Harms, H. Quantification of polymer interactions in bacterial adhesion. *Environ. Sci. Technol.* **1998**, *32*, 2909–2915.
- (46) Chia, T. W. R.; Nguyen, V. T.; McMeekin, T.; Fegan, N.; Dykes, G. A. Stochasticity of bacterial attachment and its predictability by the extended derjaguin-landau-verwey-overbeek theory. *Appl. Environ. Microb.* **2011**, *77*, 3757–3764.
- (47) Fairbrother, F.; Stubbs, A. E. 119. Studies in electro-endosmosis. Part VI. The "bubble-tube" method of measurement. *J. Chem. Soc.* **1935**, 527–529.
- (48) Wong, H.; Radke, C. J.; Morris, S. The motion of long bubbles in polygonal capillaries. Part 1. Thin films. *J. Fluid Mech.* **1995**, *292*, 71–94.

- (49) Chen, H.; Meng, Q.; Li, J. Thin lubrication film around moving bubbles measured in square microchannels. *Appl. Phys. Lett.* **2015**, *107*, 141608.
- (50) Cubaud, T.; Ho, C.-M. Transport of bubbles in square microchannels. *Phys. Fluid* **2004**, *16*, 4575–4585.
- (51) Jose, B. M.; Cubaud, T. Formation and dynamics of partially wetting droplets in square microchannels. *RSC Adv.* **2014**, *4*, 14962–14970.
- (52) Kheshgi, H. S.; Scriven, L. Dewetting: Nucleation and growth of dry regions. *Chem. Eng. Sci.* **1991**, *46*, 519 – 526.

Graphical TOC Entry

